AMERICAN SOCIETY FOR MICROBIOLOGY | Applied and Environmental Microbiology®

ENVIRONMENTAL MICROBIOLOGY

Deep-Sea Bacterium *Shewanella piezotolerans* WP3 Has Two Dimethyl Sulfoxide Reductases in Distinct Subcellular Locations

Lei Xiong,[a] Huahua Jian,[a] Xiang Xiao[a,b]

State Key Laboratory of Microbial Metabolism, School of Life Sciences and Biotechnology, Shanghai Jiao Tong University, Shanghai, People's Republic of China[a]; State Key Laboratory of Ocean Engineering, School of Naval Architecture, Ocean and Civil Engineering, Shanghai Jiao Tong University, Shanghai, People's Republic of China[b]

ABSTRACT Dimethyl sulfoxide (DMSO) acts as a substantial sink for dimethyl sulfide (DMS) in deep waters and is therefore considered a potential electron acceptor supporting abyssal ecosystems. *Shewanella piezotolerans* WP3 was isolated from west Pacific deep-sea sediments, and two functional DMSO respiratory subsystems are essential for maximum growth of WP3 under *in situ* conditions (4°C/20 MPa). However, the relationship between these two subsystems and the electron transport pathway underlying DMSO reduction by WP3 remain unknown. In this study, both DMSO reductases (type I and type VI) in WP3 were found to be functionally independent despite their close evolutionary relationship. Moreover, immunogold labeling of DMSO reductase subunits revealed that the type I DMSO reductase was localized on the outer leaflet of the outer membrane, whereas the type VI DMSO reductase was located within the periplasmic space. CymA, a cytoplasmic membrane-bound tetraheme *c*-type cytochrome, served as a preferential electron transport protein for the type I and type VI DMSO reductases, in which type VI accepted electrons from CymA in a DmsE- and DmsF-independent manner. Based on these results, we proposed a core electron transport model of DMSO reduction in the deep-sea bacterium *S. piezotolerans* WP3. These results collectively suggest that the possession of two sets of DMSO reductases with distinct subcellular localizations may be an adaptive strategy for WP3 to achieve maximum DMSO utilization in deep-sea environments.

IMPORTANCE As the dominant methylated sulfur compound in deep oceanic water, dimethyl sulfoxide (DMSO) has been suggested to play an important role in the marine biogeochemical cycle of the volatile anti-greenhouse gas dimethyl sulfide (DMS). Two sets of DMSO respiratory systems in the deep-sea bacterium *Shewanella piezotolerans* WP3 have previously been identified to mediate DMSO reduction under *in situ* conditions (4°C/20 MPa). Here, we report that the two DMSO reductases (type I and type VI) in WP3 have distinct subcellular localizations, in which type I DMSO reductase is localized to the exterior surface of the outer membrane and type VI DMSO reductase resides in the periplasmic space. A core electron transport model of DMSO reduction in WP3 was constructed based on genetic and physiological data. These results will contribute to a comprehensive understanding of the adaptation mechanisms of anaerobic respiratory systems in benthic microorganisms.

KEYWORDS *Shewanella*, DMSO respiration, electron transfer, subcellular localization, environmental adaptation

Received 6 June 2017 **Accepted** 30 June 2017

Accepted manuscript posted online 7 July 2017

Citation Xiong L, Jian H, Xiao X. 2017. Deep-sea bacterium *Shewanella piezotolerans* WP3 has two dimethyl sulfoxide reductases in distinct subcellular locations. Appl Environ Microbiol 83:e01262-17. https://doi.org/10.1128/AEM.01262-17.

Editor Shuang-Jiang Liu, Chinese Academy of Sciences

Address correspondence to Xiang Xiao, xoxiang@sjtu.edu.cn.

Dimethyl sulfoxide (DMSO) is an abundant but poorly understood methylated sulfur compound in the marine environment (1). It is thought to be an environmentally significant compound due to the potential role that it plays in the biogeochemical cycle of the climatically active gas dimethyl sulfide (DMS) (2). DMSO can be produced through the transformation of DMS by both photooxidation and biooxidation routes or by direct production from marine phytoplankton (3–5). The formation of DMSO would therefore lead to the removal of DMS from seawater, effectively controlling DMS flux into the atmosphere (2, 5). In addition to its roles in protecting cells against photogenerated oxidants and cryogenic damage, DMSO can also be used as an alternative electron acceptor for energy conservation through microbial dissimilatory reduction (6, 7). Previous studies demonstrated that DMSO acts as a substantial sink for DMS in deep oceanic waters (8, 9). Although some culturable bacteria isolated from deep-sea environments have also shown the capacity to grow anaerobically with DMSO as the sole electron acceptor (10, 11), few data are available on the electron transport pathway underlying DMSO-induced reduction by bathypelagic microorganisms.

Electron transport pathways of anaerobic DMSO respiration have been established, particularly in *Escherichia coli* (12). In *E. coli*, the *dmsABC* gene cluster encodes the following three functional proteins: DmsA, a molybdopterin (MPT) cofactor-containing catalytic subunit of DMSO reductase; DmsB, an electron transfer subunit; and DmsC, a membrane anchor subunit. These three subunits constitute a functional DMSO reductase, which is anchored to the periplasmic side of the inner membrane by DmsC (13). The electron released by menaquinol oxidation by DmsC is transferred via a series of [4Fe-4S] clusters in DmsB to the active site of DmsA, where DMSO is reduced to DMS (14).

Shewanella is a genus of facultatively anaerobic, Gram-negative gammaproteobacteria widely distributed in aquatic and sedimentary systems (15). The hallmark of *Shewanella* is its capacity to respire a diverse array of electron acceptors, making it a potential candidate for the bioremediation of pollutants (16). In *Shewanella* species, the DMSO respiratory pathway has been established only in *Shewanella oneidensis* MR-1, a strain that was isolated from the sediments of Oneida Lake in New York (17). In contrast to *E. coli*, the DMSO reductase complex in MR-1 resides on the outer leaflet of the outer membrane, with DmsE as a periplasmic electron shuttle delivering electrons from the inner membrane-bound quinol dehydrogenase, CymA, to the outer membrane DMSO reductase (18, 19).

Shewanella piezotolerans WP3 was isolated from west Pacific deep-sea sediments at a water depth of 1,914 m (20). Our previous study demonstrated that two functional DMSO respiratory subsystems were responsible for the maximum growth of WP3 under *in situ* conditions (4°C/20 MPa) (21). However, the electron transport pathway underlying DMSO-induced reduction by WP3 remains unknown. Here, we show that the two DMSO reductases (type I and type VI) in WP3 are functionally independent despite their close evolutionary relationship. Immunogold labeling of DMSO reductase subunits revealed that the type I DMSO reductase was localized on the outer leaflet of the outer membrane, whereas the type VI DMSO reductase was located within the periplasmic space. Moreover, CymA served as a preferential electron transport protein for the type I and type VI DMSO reductases, in which type VI accepted electrons from CymA in a DmsE- and DmsF-independent manner. The possession of two sets of DMSO respiratory subsystems with distinct subcellular localizations is suggested to be an adaptive strategy for WP3 to achieve maximum DMSO utilization in deep-sea environments.

RESULTS

Type VI and type I DMSO reductases are closely evolutionarily related. Bioinformatic analyses identified 24 *dms* gene clusters in 13 of 24 fully sequenced *Shewanella* strains. The copy number of the *dms* gene cluster diverged significantly among these species (Table 1). Based on the classification principle of the DMSO respiratory subsystem (16), the 24 *dms* gene clusters from 13 *Shewanella* strains were divided into 6 subsystems (Fig. 1A). Type I existed in all 13 fully sequenced *Shewanella* strains and

TABLE 1 The *dms* gene clusters are present in 13 of the 24 fully sequenced *Shewanella* strains

Strain	Geographical origin	Isolation site characteristics	Reference	No. of *dms* operon copies
S. baltica OS195	Baltic Sea (57°N, 20°E)	Seawater; anoxic basin; 140 m	54	1
S. baltica OS678	Baltic Sea (57°N, 20°E)	Seawater; low-oxygen zone; 110 m	55	1
Shewanella sp. MR-4	Black Sea	Seawater; oxic zone; 16°C; 5 m	56	1
Shewanella sp. MR-7	Black Sea	Seawater; anoxic zone; high NO_3; 60 m	56	1
S. woodyi ATCC 51908	Alboran Sea (35°N, 2°W)	Detritus; 370 m	57	1
S. putrefaciens CN-32	Albuquerque, NM, USA	Subsurface; shale sandstone; 250 m	58	1
S. frigidimarina NCIMB 400	Coast of Aberdeen, United Kingdom	Seawater; North Sea	59	2
S. halifaxensis HAW-EB4	Emerald Basin, offshore Halifax Harbor, Canada	Sediment; munitions dumping area; 215 m	60	2
S. oneidensis MR-1	Oneida Lake, NY, USA	Anaerobic sediment; Mn(IV) reduction	61	2
S. pealeana ATCC 700345	Woods Hole Harbor, MA, USA	Squid nidamental gland	62	2
S. piezotolerans WP3	West Pacific Ocean (142°E, 8°N)	Sediment; 1,914 m	11	2
S. putrefaciens 200	Alberta, Canada	Crude-oil pipeline	63	2
S. sediminis HAW-EB3	Halifax Harbor, Nova Scotia, Canada	Sediment; 50 nautical miles from shore; 215 m	64	6

matched the archetypal *dmsEFABGH* organization. Compared with the type I subsystem, types II and III each contained an additional gene predicted to encode a lipoprotein. No DmsH-encoding gene was found in the type IV subsystem, which instead contained a gene predicted to encode an endonuclease III-related protein. Type V was more characteristic of *Shimwellia*, which contains a *dmsBCAG* gene cluster (see Table S1 in the supplemental material). The type VI subsystem consisted of four genes (*dmsABGH*) and was found only in *S. piezotolerans* WP3. To investigate the evolutionary relationships of DMSO reductases among *Shewanella* strains, a phylogenetic tree containing 44 DmsA homologs (Table S1) from *Shewanella* and other gammaproteobacterial strains was constructed (Fig. 1B). The type VI DmsA homologs tended to cluster together with those of type I rather than those of other subsystems (II through V), suggesting close evolutionary relatedness between type VI and type I. Except for type VI, the subsystems (I through V) were located on distinct phylogenetic branches, and DmsA homologs from the same subsystem tended to group together.

The two DMSO reductases are functionally independent. To investigate whether the subunits from these two DMSO reductases were interchangeable, we constructed two unmarked double in-frame Δ*dmsA1* Δ*dmsB6* and Δ*dmsA6* Δ*dmsB1* deletion mutants. Physiological assays demonstrated that the two double mutants lost the ability to utilize DMSO for anaerobic growth under different conditions (Fig. 2). Moreover, transcriptional analyses revealed that deletion of the individual gene did not eliminate the expression of other genes within the same gene cluster (see Fig. S1A in the supplemental material). To confirm that the loss of DMSO-dependent growth of the Δ*dmsA1* Δ*dmsB6* and Δ*dmsA6* Δ*dmsB1* mutants can be rescued by introduction of *dmsA1* and *dmsA6*, respectively, two complemented strains (the Δ*dmsA1* Δ*dmsB6-dmsA1*-C and Δ*dmsA6* Δ*dmsB1-dmsA6*-C strains [where "-C" refers to complementation]) were generated. As expected, the introduction of either *dmsA1* into the Δ*dmsA1* Δ*dmsB6* mutant or *dmsA6* into the Δ*dmsA6* Δ*dmsB1* mutant partially restored the ability of these double mutants to utilize DMSO for anaerobic growth (Fig. S1B and C). These results suggested that the deficiencies of DMSO-dependent growth in Δ*dmsA1* Δ*dmsB6* and Δ*dmsA6* Δ*dmsB1* mutants were attributable to the inability to form functional DMSO reductases rather than to the silencing of the expression of both *dms* gene clusters. In other words, functional compensation did not occur between DmsA1 and DmsA6 or between DmsB1 and DmsB6.

Type I and type VI DMSO reductases have different subcellular localizations. To further examine the subcellular localizations of both DMSO reductases in WP3, we visualized the location of the DmsB subunits (DmsB1 and DmsB6). DmsB was monitored instead of DmsA because its localization should be DmsA dependent as only DmsA has a twin-arginine translocation (Tat) signal sequence (14). Two complemented strains of the Δ*dmsB1* Δ*dmsB6* (ΔΔ*dmsB*) mutant (the ΔΔ*dmsB-dmsB1*-3HA and ΔΔ*dmsB-dmsB6-*

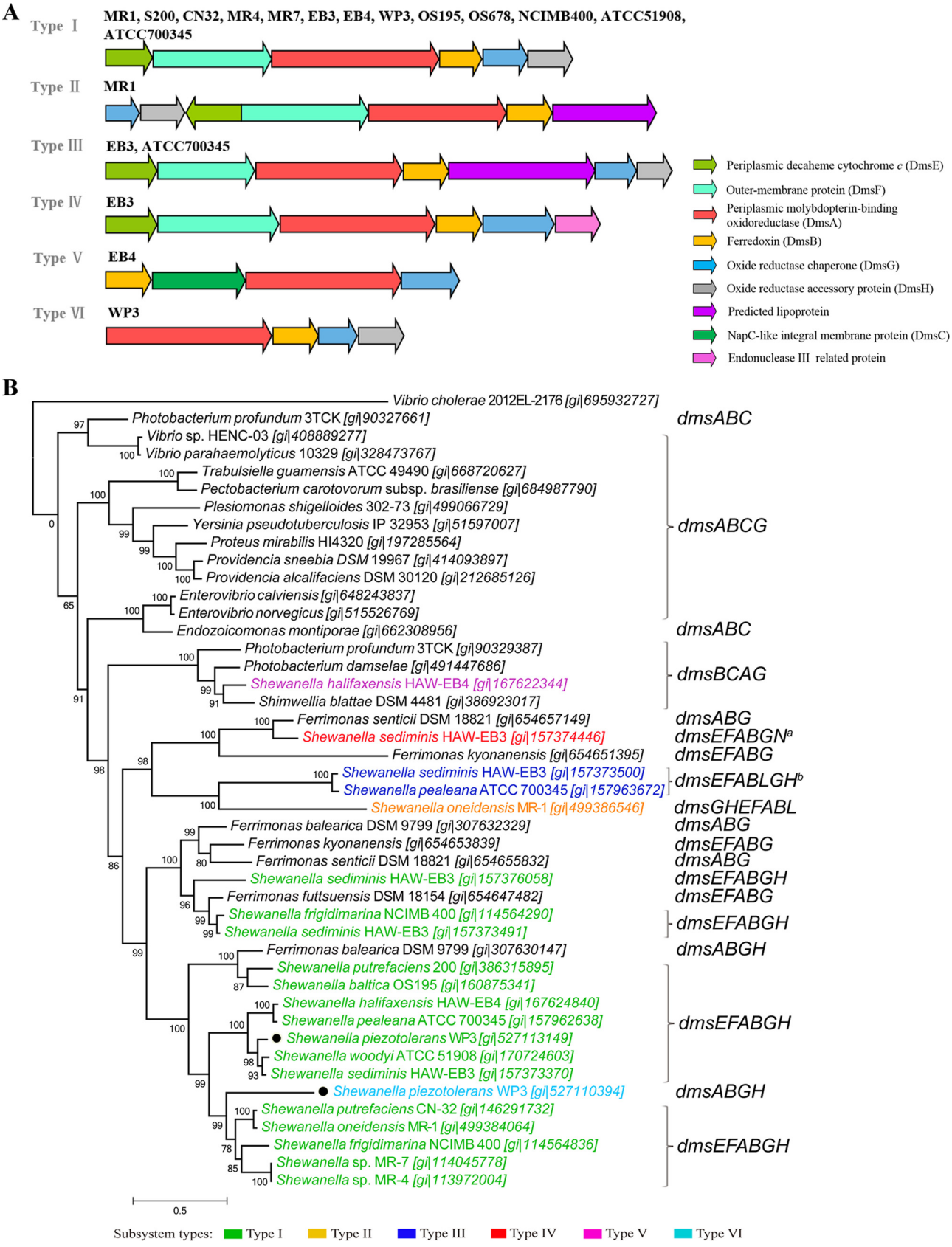

FIG 1 Classification and phylogenetic analysis of DMSO respiratory subsystems in *Shewanella* species. (A) Classification of DMSO respiratory subsystems in *Shewanella* species according to a previous report (16). Name abbreviations: MR1, *S. oneidensis* MR-1; S200, *Shewanella putrefaciens* 200; CN32, *S.*

(Continued on next page)

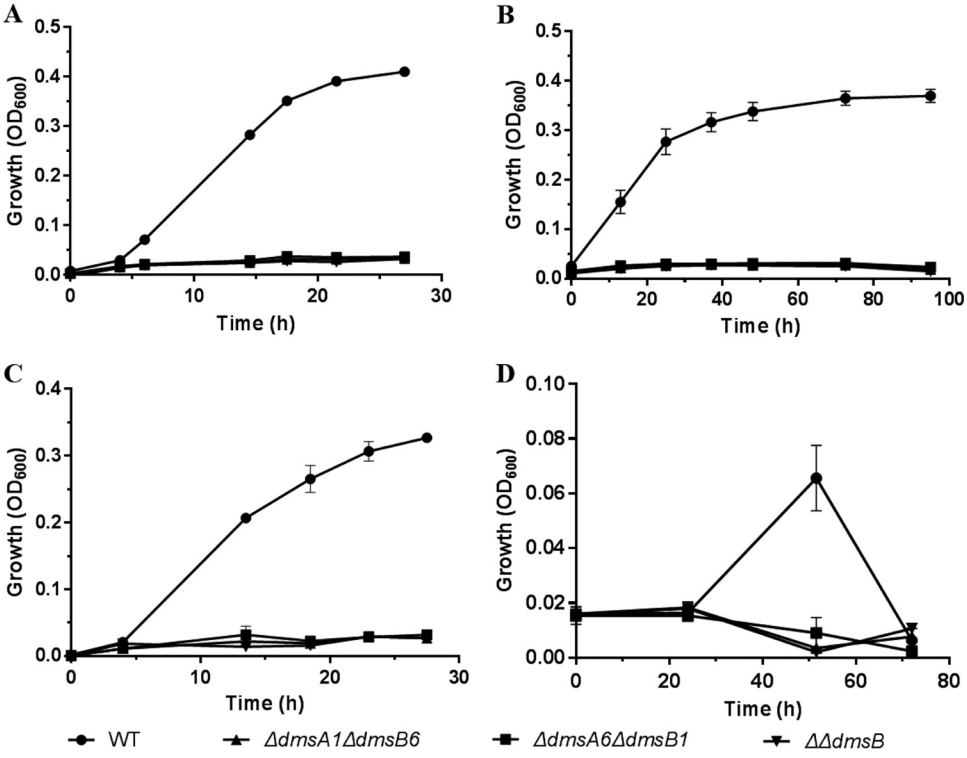

FIG 2 Growth curves of WP3 mutants at different temperatures and pressures with DMSO as the sole electron acceptor. (A) 20°C and 0.1 MPa; (B) 4°C and 0.1 MPa; (C) 20°C and 20 MPa; (D) 4°C and 20 MPa. The data shown represent the results of two independent experiments, and the error bars represent standard deviations of averages of triplicate cultures.

3HA strains) were constructed as described in Materials and Methods. Physiological assays demonstrated that both complemented strains regained the ability to utilize DMSO for anaerobic growth (see Fig. S2 in the supplemental material). To determine the subcellular localization of DmsB-HA, immunogold-labeled anti-hemagglutinin (HA) antibodies were used to probe intact cells and ultrathin sections of these two strains, and the samples were then observed by transmission electron microscopy.

Immunoelectron microscopic analysis of intact cells of these two strains grown under different conditions revealed the following: (i) under aerobic conditions, only rare gold particles were detected on the cell surface of the ΔΔ*dmsB-dmsB1*-3HA complemented strain (see Fig. S3A in the supplemental material), whereas no gold particles were detected on the cell surface of the ΔΔ*dmsB-dmsB6*-3HA complemented strain (Fig. S3C); and (ii) under anaerobic conditions, a number of gold particles were detected on the cell surface of the ΔΔ*dmsB-dmsB1*-3HA complemented strain (Fig. S3B), whereas no gold particles were detected on the cell surface of the ΔΔ*dmsB-dmsB6*-3HA complemented strain (Fig. S3D). These results implied that type I and type VI DMSO reductases had different subcellular localizations, in which the type I DMSO reductase tended to be localized extracellularly.

To further confirm their subcellular localization, ultrathin sections of the two strains grown under different conditions were analyzed by immunoelectron microscopy, which revealed the following: (i) under aerobic conditions, gold particles were scattered

FIG 1 Legend (Continued)

putrefaciens CN-32; MR4, *Shewanella* sp. MR-4; MR7, *Shewanella* sp. MR-7; EB3, *Shewanella sediminis* HAW-EB3; EB4, *Shewanella halifaxensis* HAW-EB4; WP3, *S. piezotolerans* WP3; OS195, *Shewanella baltica* OS195; OS678, *S. baltica* OS678; NCIMB400, *Shewanella frigidimarina* NCIMB 400; ATCC 51908, *Shewanella woodyi* ATCC 51908; ATCC 700345, *Shewanella pealeana* ATCC 700345. (B) Phylogenetic tree of DmsA protein sequences from *Shewanella* and other gammaproteobacteria. We used trimethylamine *N*-oxide (TMAO) reductase (TorA) of *Vibrio cholerae* 2012EL-2176 as the outgroup. The letter N in *dmsEFABGN* represents a gene encoding an endonuclease III-related protein. The letter L in *dmsEFABLGH* represents a gene encoding a lipoprotein.

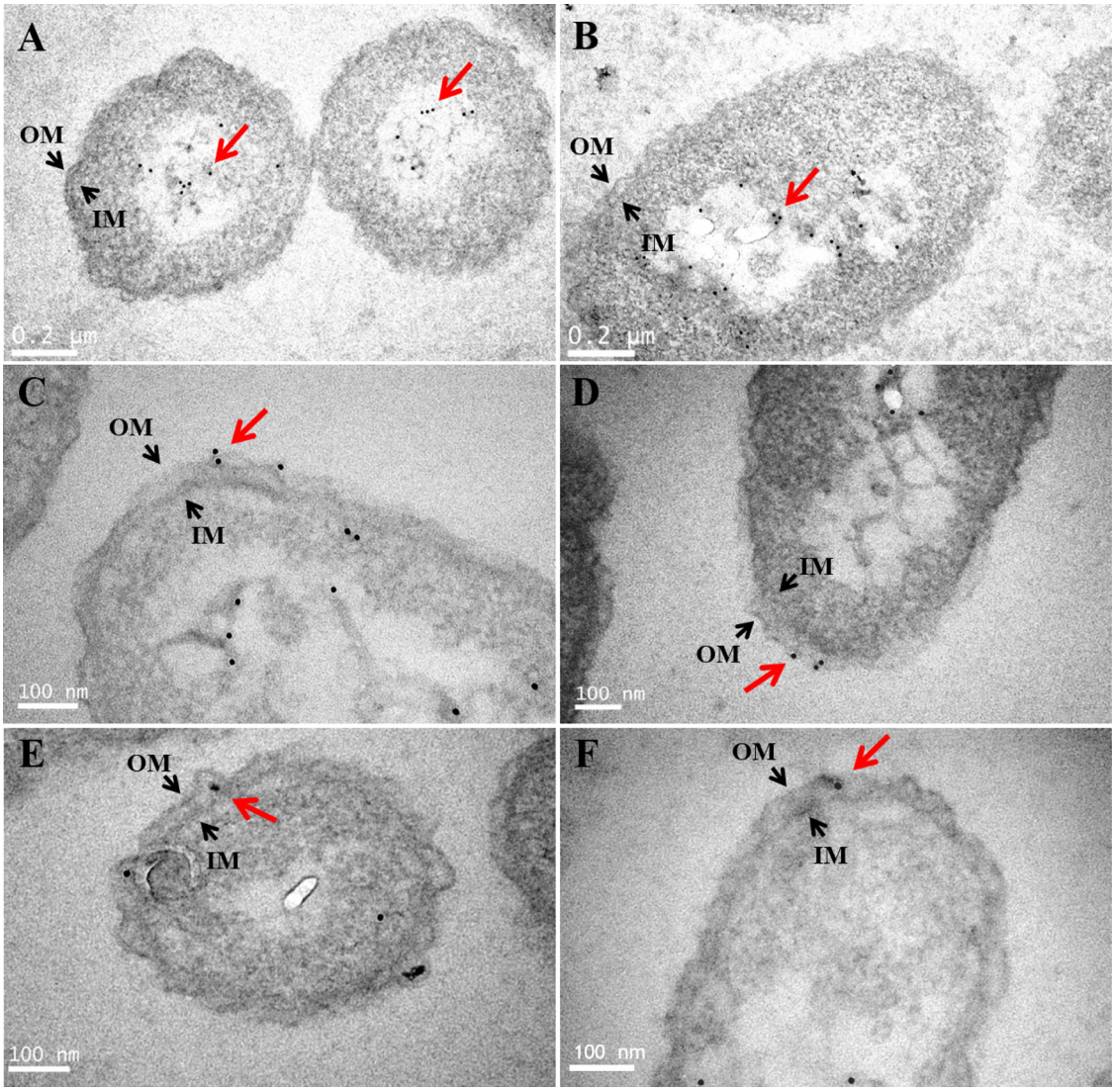

FIG 3 Immunoelectron microscopic analysis of DmsB-HA proteins in WP3 ultrathin sections. (A) Ultrathin section of the ΔΔ*dmsB-dmsB1*-3HA strain grown aerobically. (B) Ultrathin section of the ΔΔ*dmsB-dmsB6*-3HA strain grown aerobically. (C and D) Ultrathin sections of the ΔΔ*dmsB-dmsB1*-3HA strain grown anaerobically. (E and F) Ultrathin sections of the ΔΔ*dmsB-dmsB6*-3HA strain grown anaerobically. The 10-nm gold particles are indicated by red arrows, and inner membranes (IM) and outer membranes (OM) are indicated by black arrows. The white line in the lower left corner represents the image scale for transmission electron microscopy.

over the cytoplasmic matrix of both the ΔΔ*dmsB-dmsB1*-3HA (Fig. 3A) and ΔΔ*dmsB-dmsB6*-3HA (Fig. 3B) complemented strains, but no gold particles were located on the outer and inner membranes of these two strains; and (ii) under anaerobic conditions, gold particles were detected on the outer membrane of the ΔΔ*dmsB-dmsB1*-3HA complemented strain (Fig. 3C and D) but within the periplasmic space of the ΔΔ*dmsB-dmsB6*-3HA complemented strain (Fig. 3E and F), consistent with the absence of gold particles on the cell surface of the ΔΔ*dmsB-dmsB6*-3HA complemented strain (Fig. S3D). Statistical analysis revealed that the number of gold particles per field on the outer membrane or in the periplasmic space of the ΔΔ*dmsB-dmsB1*-3HA complemented strain was 1.13 ± 0.11 or 0.42 ± 0.09, respectively, whereas the number of gold particles per field on the outer membrane or in the periplasmic space of the ΔΔ*dmsB-dmsB6*-3HA complemented strain was 0.15 ± 0.05 or 1.02 ± 0.07, respectively (see Fig. S4 in the supplemental material). In contrast, negative controls in which the primary antibody was omitted showed no immunogold labeling (see Fig. S5 in the supplemental material). Taken together, these results suggested that the two sets of DMSO

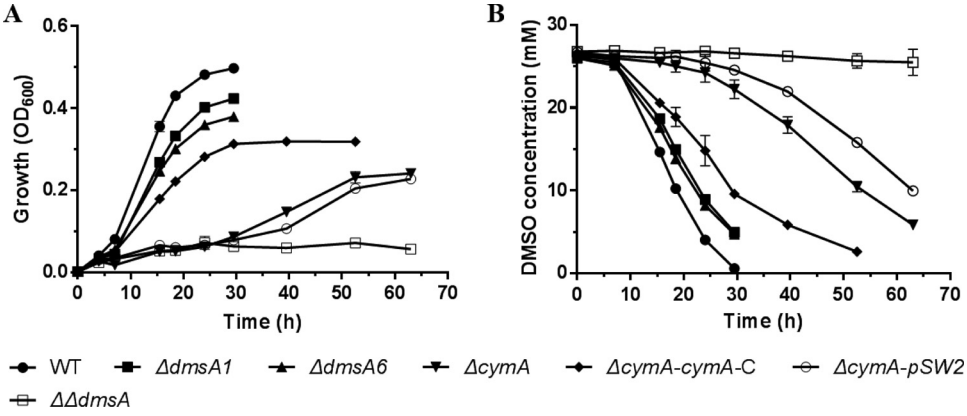

FIG 4 Growth and corresponding DMSO consumption curves of the WP3 mutants grown at 20°C/0.1 MPa in 2216E medium using DMSO as the sole electron acceptor. The data shown represent the results of two independent experiments, and the error bars represent standard deviations of averages of triplicate cultures. Δ*cymA-cymA*-C, the *cymA* gene-complemented (Δ*cymA/cymA*) strain.

reductases in WP3 had distinct subcellular localizations, in which the type VI DMSO reductase was located within the periplasmic space whereas the type I DMSO reductase was localized on the outer leaflet of the outer membrane.

CymA is the preferential electron transport protein for DMSO reductases in WP3. CymA, a cytoplasmic membrane-anchored tetraheme *c*-type cytochrome, plays a central role in anaerobic respiration by transferring electrons from the menaquinol pool to a variety of terminal reductases (18). To investigate whether the two DMSO respiratory systems of WP3 obtain electrons from CymA, the Δ*cymA* mutant was developed. Growth assays demonstrated that wild-type WP3 and Δ*dmsA1* and Δ*dmsA6* mutant strains propagated with a high growth rate when grown in a DMSO medium at 20°C and reached stationary phase within 20 h, whereas strains lacking *cymA* were severely deficient in DMSO-dependent growth and exhibited a relatively long lag phase (Fig. 4). In contrast, the *cymA* gene-complemented (Δ*cymA/cymA*) strain exhibited a restored ability to immediately respire DMSO for anaerobic growth. These results collectively indicated that CymA serves as a preferential electron transport protein for both the type I and type VI DMSO respiratory subsystems in WP3.

DmsE passes electrons to DmsA1 for DMSO reduction. DmsE is the paralogue of MtrA, a periplasmic decaheme *c*-type cytochrome involved in iron oxide reduction in *S. oneidensis* MR-1 (18, 22). A rough model for DMSO reduction in *Shewanella* has been proposed in which the periplasmic DmsE mediates electron transfer from CymA to the terminal DMSO reductase (19). To investigate the role of DmsE in DMSO respiration in WP3, three in-frame deletion mutants (the Δ*dmsE*, Δ*dmsA1* Δ*dmsE*, and Δ*dmsA6* Δ*dmsE* mutant strains) were constructed. Growth assays demonstrated that all of these mutants showed growth deficiencies in anaerobic DMSO respiration of various degrees (Fig. 5A). The cell density of the Δ*dmsE* mutant at stationary phase was slightly lower than that of the wild-type strain but higher than those of the other mutants, including the Δ*dmsA1* and Δ*dmsA6* mutant strains. Interestingly, there was no apparent difference in cell density between the Δ*dmsA1* Δ*dmsE* and Δ*dmsA1* mutants, whereas the cell density of the Δ*dmsA6* Δ*dmsE* mutant was significantly lower than that of the Δ*dmsA6* mutant. In addition, culture medium was collected at different time points, filtered, and analyzed to calculate DMSO consumption by these strains (Fig. 5B). The high-performance liquid chromatography (HPLC) results showed that the amount of DMSO utilized by the Δ*dmsA1* Δ*dmsE* mutant strain was nearly equivalent to that utilized by the Δ*dmsA1* mutant strain. Compared with the Δ*dmsA6* mutant, the Δ*dmsA6* Δ*dmsE* mutant exhibited a more severe deficiency in DMSO reduction. Collectively, these results suggested that the type VI DMSO reductase accepted electrons from CymA in a DmsE-independent manner. However, the type I DMSO reductase was strongly dependent on DmsE for electron transfer.

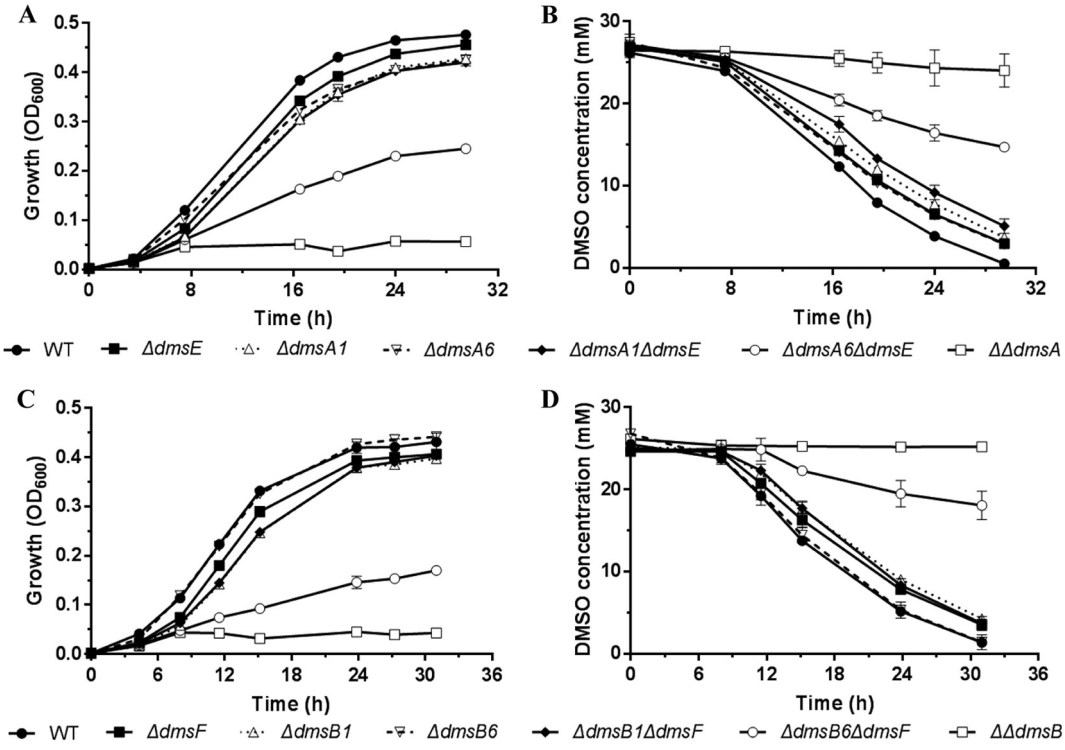

FIG 5 Growth and corresponding DMSO consumption curves of the WP3 mutants grown at 20°C/0.1 MPa in 2216E medium using DMSO as the sole electron acceptor. The data shown represent the results of two independent experiments, and the error bars represent standard deviations of averages of triplicate cultures.

DmsF facilitates electron transfer between the type I DMSO reductase and DmsE. DmsF, an integral outer membrane β-barrel protein, facilitates electron transfer by forming a pore-like structure through the outer membrane to mediate direct interaction between the extracellular DMSO reductase and DmsE (23–25). To investigate the role of DmsF in DMSO respiration in WP3, three in-frame deletion mutants (the Δ*dmsF*, Δ*dmsB1* Δ*dmsF*, and Δ*dmsB6* Δ*dmsF* mutant strains) were generated. Growth assays demonstrated that the cell density of the Δ*dmsF* mutant at stationary phase was slightly lower than that of the Δ*dmsB6* mutant but equivalent to that of the Δ*dmsB1* mutant (Fig. 5C). As expected, there was no apparent difference in cell density between the Δ*dmsB1* and Δ*dmsB1* Δ*dmsF* mutants, whereas the cell density of the Δ*dmsB6* Δ*dmsF* mutant was significantly lower than that of the Δ*dmsB6* mutant. In addition, the HPLC results showed that the amount of DMSO utilized by the Δ*dmsB1* Δ*dmsF* mutant was nearly equivalent to that utilized by the Δ*dmsB1* mutant (Fig. 5D). Compared with that of the Δ*dmsB6* mutant, the Δ*dmsB6* Δ*dmsF* mutant strain exhibited a more severe deficiency in DMSO reduction. To further support the notion that DmsF is responsible for targeting the type I DMSO reductase to the outer leaflet of the outer membrane, a complemented strain of the Δ*dmsB1* Δ*dmsF* mutant (the Δ*dmsB1* Δ*dmsF-dmsB1*-3HA strain) was also constructed. To determine the subcellular localization of DmsB1-HA, ultrathin sections of this strain grown under anaerobic conditions were analyzed by immunoelectron microscopy (data not shown). Statistical analysis revealed that the number of gold particles per field on the outer membrane or in the periplasmic space of the Δ*dmsB1* Δ*dmsF-dmsB1*-3HA complemented strain was 0.29 $\pm$ 0.09 or 0.32 $\pm$ 0.08, respectively, indicating that the deletion of *dmsF* resulted in a decreased accumulation of type I DMSO reductase to the outer membrane (Fig. S4). Collectively, these results suggested that DmsF was dispensable for electron transfer between the type VI DMSO reductase and CymA. However, DmsF played an important role in facilitating electron transfer between the type I DMSO reductase and DmsE.

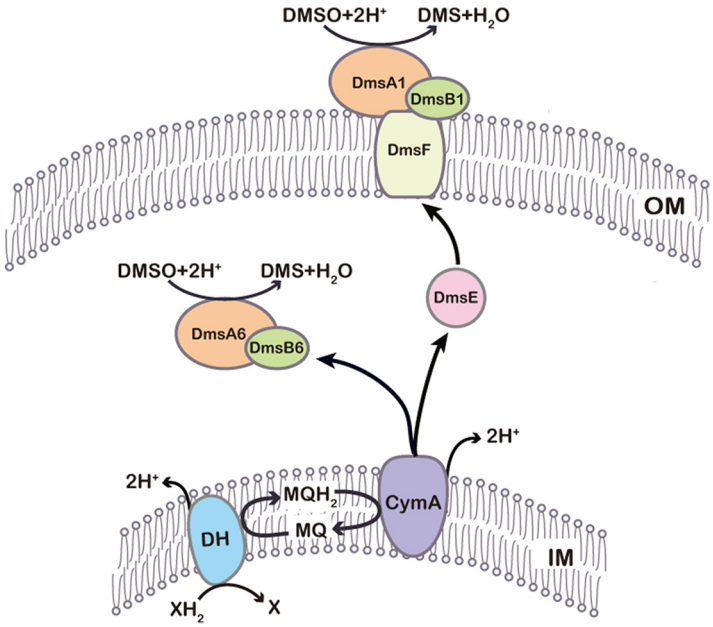

FIG 6 The core electron transport model of two sets of DMSO respiratory systems in the deep-sea bacterium *S. piezotolerans* WP3. Inner membrane-bound dehydrogenases (DH) donate electrons through the lipophilic menaquinone pool to CymA where they are passed to the type I and type VI DMSO reductases. The type I DMSO reductase resides on the outer leaflet of the outer membrane and, thus, relies on DmsE as an electron shuttle delivering electrons from CymA to the outer membrane DMSO reductase. The type VI DMSO reductase is located within the periplasmic space and is capable of obtaining electrons from CymA in a DmsE-independent manner. The trilaminar cell envelope of Gram-negative bacteria is composed of the inner membrane (IM), outer membrane (OM), and the periplasm between the IM and OM. DH, dehydrogenase; XH_2, electron donors; MQ, menaquinone; MQH_2, menaquinol.

DISCUSSION

Based on the data presented above and the current understanding of anaerobic DMSO respiration, we propose a core electron transport model of DMSO respiration in *S. piezotolerans* WP3 (Fig. 6). The dehydrogenases (DHs) located at the head end of the electron transport chain catalyze the oxidation of electron donors (XH_2), contributing to proton gradient generation and the reduction of menaquinone (26). The reduced menaquinone transfers electrons to the inner membrane-bound quinol dehydrogenase CymA, which in turn donates electrons to both the type I and type VI DMSO reductases. The type I DMSO reductase resides on the outer leaflet of the outer membrane and is unable to receive electrons from CymA directly, and the periplasmic decaheme *c*-type cytochrome DmsE serves as an electron shuttle delivering electrons from CymA to the outer membrane DMSO reductase. The integral membrane β-barrel protein, DmsF, may facilitate electron transfer by forming a pore-like structure through the outer membrane to mediate direct interaction between the type I DMSO reductase and DmsE (19, 27, 28). The type VI DMSO reductase is located within the periplasmic space and is capable of obtaining electrons from CymA in a DmsE- and DmsF-independent manner. In contrast, the DMSO reductase in *E. coli* is anchored to the periplasmic side of the inner membrane by DmsC. The electron released by menaquinol oxidation by DmsC is transferred via the [4Fe-4S] clusters in DmsB to the active site of DmsA (14, 29). In *S. oneidensis* MR-1, the DMSO reductase resides on the outer leaflet of the outer membrane, with DmsE as a periplasmic electron shuttle delivering electrons from the inner membrane-bound quinol dehydrogenase CymA to the outer membrane DMSO reductase (19). By combining these results, we conclude that the DMSO respiratory pathway in the deep-sea bacterium *S. piezotolerans* WP3 is more complex than those previously reported in other strains (12, 19).

CymA serves as a preferential electron transport protein for the type I and type VI

DMSO respiratory subsystems in WP3 (Fig. 4). In the Δ*dmsA1* mutant, although DmsE can accept electrons from CymA, the electrons carried by DmsE cannot be further consumed by the type I DMSO reductase due to the deficiency of the type I DMSO respiratory subsystem. However, the type VI DMSO respiratory subsystem in the Δ*dmsA1* mutant can still accept electrons from CymA and function in DMSO reduction, and thus this strain can grow anaerobically in DMSO medium. In the Δ*dmsA6* mutant, although the type VI DMSO respiratory subsystem has lost its function, the type I DMSO respiratory subsystem can still accept electrons from CymA, and therefore the Δ*dmsA6* mutant can also grow anaerobically in the same medium. Moreover, we observed that the Δ*cymA* mutant exhibited no apparent growth in DMSO medium until after approximately 20 h of incubation (Fig. 4), implying that the DMSO reductases in WP3 can also accept electrons from the quinol pool in an alternative electron transfer pathway independent of CymA. In *S. oneidensis* MR-1, it was reported that a quinol dehydrogenase complex (SirCD) can functionally replace the *c*-type cytochrome, CymA, in several respiratory pathways, including fumarate, DMSO, and ferric citrate (30). Genetic analyses revealed that the expression of *sirCD* genes in MR-1 Δ*cymA* suppressor mutants is mediated by an insertion sequence (30). Using a bioinformatics approach, genes (*swp4653* and *swp4652*) encoding SirC and SirD homologs were also identified in the WP3 genome. Transcriptional analysis demonstrated that, compared with those of the WP3 wild type (WT), the expression profiles of *sirC* and *sirD* in the Δ*cymA* mutant were significantly induced under the same conditions (our unpublished data). Based on these results, we propose that the SirCD complex in WP3 may play a minor role in DMSO-dependent growth in the absence of CymA. Considering that CymA is a member of the NapC/NirT family (24, 25), other subgroups, such as NapC, NrfH, and NirT, may also exert similar functions.

To evaluate the impact of *dmsE* deletion on growth, we calculated the DMSO consumption of the WP3 mutants by standardizing the growth yield to the same cell density (see Fig. S6 in the supplemental material). Our data showed that the Δ*dmsA1* Δ*dmsE* mutant required the same amount of DMSO as the WP3 WT to reach the same growth under the tested conditions (20°C/0.1 MPa), further supporting the conclusion that the type VI DMSO respiratory subsystem in WP3 is DmsE independent. However, DmsE in the Δ*dmsA1* mutant may dissipate electrons of the quinol pool via CymA (31), resulting in a decrease in the amount of electrons available for the type VI DMSO reductase. Although the Δ*dmsA6* Δ*dmsE* mutant required the same amount of DMSO as the Δ*dmsA6* mutant to reach the same growth (Fig. S6), the Δ*dmsA6* Δ*dmsE* mutant showed a more severe growth deficiency in DMSO medium (Fig. 5A and B), suggesting that either other periplasmic electron shuttles functionally replace DmsE in the context of DMSO reduction or the type I DMSO reductase has some activity in the periplasm (obtaining electrons from CymA). A previous study focusing on *S. oneidensis* MR-1 demonstrated that, in addition to DmsE, CctA (a tetraheme *c*-type cytochrome) was also able to transfer electrons from CymA to the DMSO reductase, and the Δ*dmsE* Δ*cctA* double mutant grew significantly slower than either the Δ*dmsE* mutant or Δ*cctA* mutant in anaerobic DMSO medium (18). Collectively, these results suggest that functional redundancy and plasticity may be common features of *Shewanella* in electron transport to DMSO.

DMSO is generally thought to be a soluble organic compound that is highly permeable to biological membranes (32). Therefore, the periplasmic localization of DMSO reductases in *E. coli* and *Rhodobacter* is not surprising (14, 33). The *dms* gene cluster (*dmsABC*) in *E. coli* is more characteristic of the type V subsystem, which encodes three functional proteins, DmsA, DmsB, and DmsC. As it lacks genes that encode the DmsEF module and CymA, the integral membrane protein DmsC is required to anchor the DMSO reductase complex (DmsAB) to the membrane and for quinol oxidation (34). In *Rhodobacter*, the DMSO reductase operon consists of three genes (*dorCAD*), which encode three functional proteins, DorC (the NapC-like integral membrane anchor), DorD (the DMSO reductase-specific chaperone), and DorA (the periplasmic DMSO reductase). DorA proteins differ from DmsA proteins in that they do not contain

iron-sulfur clusters. The Dor-type DMSO reductases are soluble and only transiently interact with the membrane-bound DorC-type cytochromes that act as electron donors for these systems (34). In *Shewanella* species, DMSO respiration was first characterized in *S. oneidensis* MR-1, in which the DMSO reductase is localized on the outer leaflet of the outer membrane (19). Here, we observed that *S. piezotolerans* WP3 had two sets of DMSO reductases; the type I DMSO reductase was localized on the outer leaflet of the outer membrane, whereas the type VI DMSO reductase was located within the periplasmic space. Moreover, the DMSO-dependent growth yield conferred by the presence of both DMSO reductases was higher than the growth yield conferred by either of the two DMSO reductases alone (21).

Why would two distinct DMSO respiratory subsystems confer *S. piezotolerans* WP3 a selective advantage for DMSO-dependent growth? Insight into this question comes from considering the typical growth environment of *Shewanella*. *S. piezotolerans* WP3 was isolated from west Pacific sediments at a depth of 1,914 m, an environment with permanently low temperature (~2°C to ~4°C) and high pressure (20 MPa). Theoretically, low temperature and high pressure in deep-sea environments can decrease the fluidity of lipids and thus depress the functions of biological membranes (35, 36), resulting in decreased diffusion of DMSO into the cell (37, 38). To survive and proliferate under such conditions, WP3 may have evolved DMSO respiration subsystems in which the type I DMSO reductase allows WP3 to more efficiently utilize DMSO dispersed in the extracellular environment, whereas the type VI DMSO reductase enables WP3 to utilize DMSO penetrating the periplasmic space. Consistent with this idea, it has been reported that the expression of the type I *dms* gene cluster at 4°C was significantly induced with increasing pressure from atmospheric pressure to high-pressure (10 and 20 MPa) conditions, whereas the expression of the type VI *dms* gene cluster was greatly reduced under the same conditions (21). Taken together, the two sets of DMSO reductases with distinct subcellular localizations may represent an adaptive strategy for WP3 to achieve maximum DMSO utilization in deep-sea environments.

DmsA1 shares high sequence similarity with DmsA6 (54%), and DmsB1 shares high sequence similarity with DmsB6 (56%). However, the type I and type VI DMSO reductases in WP3 displayed distinct subcellular localizations (Fig. 3; see also Fig. S3 in the supplemental material). Previous studies have demonstrated that type II secretion systems (T2SSs) are required for the proper extracellular localization of both DMSO reductase and metal reductase in *Shewanella* species (19, 39, 40). Based on these data, we propose that T2SS may be involved in the secretion of type I DMSO reductase rather than type VI DMSO reductase. T2SSs are molecular machines that promote the specific transport of folded periplasmic proteins in Gram-negative bacteria, but the T2SS secretion signal remains a mystery (41, 42). In general, exoproteins tend to be rich in β-strands, and this is also true of the exoproteins that are secreted by the T2SS according to currently available structures (42, 43). Further investigations into these two DMSO reductases at the sequence or structural level may provide insights into the molecular mechanism of protein sorting by T2SS.

In conclusion, we have demonstrated that the two DMSO reductases (type I and type VI) in WP3 are functionally independent despite their close evolutionary relationship. Both DMSO reductases in WP3 had distinct subcellular localizations, in which the type I DMSO reductase was localized on the outer leaflet of the outer membrane and the type VI DMSO reductase was located within the periplasmic space. CymA served as a preferential electron transport protein for the type I and type VI DMSO reductases. Based on these data, we proposed a core electron transport model of DMSO respiration in the deep-sea bacterium *S. piezotolerans* WP3. Moreover, possession of two sets of DMSO reductases with distinct subcellular localizations is likely to be an adaptive strategy for WP3 to achieve maximum DMSO utilization in deep-sea environments.

MATERIALS AND METHODS

Bacterial strains and growth conditions. The bacterial strains used in this study are listed in Table 2. *E. coli* strain WM3064 was routinely grown in Luria broth (LB) media at 37°C with the addition of 500

TABLE 2 Bacterial strains and plasmids used in this study

Strain or plasmid	Description	Reference or source
E. coli		
WM3064	Donor strain for conjugation; Δ*dapA*	65
S. piezotolerans WP3		
WT	Wild-type strain	Lab stock
Δ*dmsA1* mutant	*dmsA1* single mutant derived from WP3	Lab stock
Δ*dmsB1* mutant	*dmsB1* single mutant derived from WP3	Lab stock
Δ*dmsA6* mutant	*dmsA6* single mutant derived from WP3	Lab stock
Δ*dmsB6* mutant	*dmsB6* single mutant derived from WP3	Lab stock
Δ*dmsE* mutant	*dmsE* single mutant derived from WP3	This study
Δ*dmsF* mutant	*dmsF* single mutant derived from WP3	This study
Δ*cymA* mutant	*cymA* single mutant derived from WP3	Lab stock
ΔΔ*dmsA* mutant	*dmsA1* and *dmsA6* double mutant derived from WP3	This study
ΔΔ*dmsB* mutant	*dmsB1* and *dmsB6* double mutant derived from WP3	Lab stock
Δ*dmsA1* Δ*dmsB6* mutant	*dmsA1* and *dmsB6* double mutant derived from WP3	This study
Δ*dmsA6* Δ*dmsB1* mutant	*dmsA6* and *dmsB1* double mutant derived from WP3	This study
Δ*dmsA1* Δ*dmsE* mutant	*dmsA1* and *dmsE* double mutant derived from WP3	This study
Δ*dmsA6* Δ*dmsE* mutant	*dmsA6* and *dmsE* double mutant derived from WP3	This study
Δ*dmsB1* Δ*dmsF* mutant	*dmsB1* and *dmsF* double mutant derived from WP3	This study
Δ*dmsB6* Δ*dmsF* mutant	*dmsB6* and *dmsF* double mutant derived from WP3	This study
Δ*cymA*/*cymA* strain	Complemented strain of Δ*cymA* single mutant with *cymA*	This study
Δ*cymA*-pSW2 strain	Δ*cymA* containing the empty pSW2 vector as negative control	This study
ΔΔ*dmsB*-*dmsB1*-3HA strain	Complemented strain of ΔΔ*dmsB* double mutant with *dmsB1*-3HA	This study
ΔΔ*dmsB*-*dmsB6*-3HA strain	Complemented strain of ΔΔ*dmsB* double mutant with *dmsB6*-3HA	This study
Δ*dmsB1* Δ*dmsF*-*dmsB1*-3HA strain	Complemented strain of Δ*dmsB1* Δ*dmsF* double mutant with *dmsB1*-3HA	This study
Δ*dmsA1* Δ*dmsB6*-*dmsA1*-C strain	Complemented strain of Δ*dmsA1* Δ*dmsB6* double mutant with wild-type *dmsA1*	This study
Δ*dmsA6* Δ*dmsB1*-*dmsA6*-C strain	Complemented strain of Δ*dmsA6* Δ*dmsB1* double mutant with wild-type *dmsA6*	This study
Δ*dmsA1* Δ*dmsB6*-pSW2 strain	Δ*dmsA1* Δ*dmsB6* double mutant containing the empty pSW2 vector as negative control	This study
Δ*dmsA6* Δ*dmsB1*-pSW2 strain	Δ*dmsA6* Δ*dmsB1* double mutant containing the empty pSW2 vector as negative control	This study
Plasmid		
pSW2	Chloramphenicol resistance, generated from filamentous bacteriophage SW1; used for complementation	48
pSW2-*dmsA1*	pSW2 containing *dmsA1* and the promoter region of *dmsA6*	Lab stock
pSW2-*dmsA6*	pSW2 containing *dmsA6* and its own promoter region	Lab stock
pSW2- *dmsB1*-3HA	pSW2 containing *dmsB1*-3HA and the promoter region of *dmsB6*	This study
pSW2- *dmsB6*-3HA	pSW2 containing *dmsB6*-3HA and its own promoter region	This study
pSW2-*cymA*	pSW2 containing *cymA* and its own promoter region	This study
pRE112	Chloramphenicol resistance, suicide plasmid with *sacB1* gene as a negative selection marker; used for gene deletion	Lab stock
pRE112-Δ*dmsA1*	pRE112 containing the PCR fragment for deleting *dmsA1*	Lab stock
pRE112-Δ*dmsB1*	pRE112 containing the PCR fragment for deleting *dmsB1*	Lab stock
pRE112-Δ*dmsA6*	pRE112 containing the PCR fragment for deleting *dmsA6*	Lab stock
pRE112-Δ*dmsB6*	pRE112 containing the PCR fragment for deleting *dmsB6*	Lab stock
pRE112-Δ*dmsE*	pRE112 containing the PCR fragment for deleting *dmsE*	This study
pRE112-Δ*dmsF*	pRE112 containing the PCR fragment for deleting *dmsF*	This study
pRE112-Δ*cymA*	pRE112 containing the PCR fragment for deleting *cymA*	Lab stock

μM 2,6-diaminopimelic acid (DAP) (Sigma-Aldrich, St. Louis, Mo, USA). For aerobic growth, *S. piezotolerans* WP3 strains were cultured in 2216E broth (44, 45) with minor modification (5 g liter^{-1} tryptone, 1 g liter^{-1} yeast extract, 34 g liter^{-1} NaCl) at 20°C on a rotary shaker at 220 rpm. If necessary, chloramphenicol was added to both media (30 μg ml^{-1} for *E. coli* strains and 10 μg ml^{-1} for WP3 strains). For anaerobic growth assays, WP3 strains were cultivated in 2216E broth supplemented with 20 mM lactate and 25 mM DMSO (21). The serum bottles containing 100 ml of fresh medium were made anaerobic by flushing with nitrogen gas through the butyl rubber stopper, which was further fixed with metal seals to strip the dissolved oxygen before autoclave sterilization. To examine high-pressure growth of WP3 strains at different temperatures, each culture was grown to stationary phase in 2216E broth at 1 atm (1 atm = 0.101 MPa) and 20°C on a rotary shaker. The late-log-phase cultures were diluted into the same medium to an optical density at 600 nm (OD_{600}) of 0.3. Aliquots of the diluted culture (1 ml) were injected into serum bottles containing 100 ml of anaerobic medium through the butyl rubber stopper. After brief shaking, 2.5-ml disposable syringes were used to distribute the culture in 2-ml aliquots. The syringes with needles were inserted into rubber stoppers in a vinyl anaerobic airlock chamber (Coy Laboratory Products Inc., Grass Lake, MI, USA). Then, the syringes were incubated at a hydrostatic pressure of 20 MPa at 4°C or 20°C in stainless steel vessels (Nantong Feiyu Science and Technology Exploitation Co., Ltd.,

China) that were pressurized using water and a hydraulic pump. These systems were equipped with quick-connect fittings for rapid decompression and recompression (23, 46).

Deletion mutagenesis and complementation. In-frame deletion mutagenesis of *dmsE* (*swp3461*) was performed as previously reported (44). The primers designed to amplify PCR products for mutagenesis are summarized in Table 3. To construct the *dmsE* in-frame deletion mutant, two fragments flanking *dmsE* were amplified by PCR. Fusion PCR products were generated using the amplified PCR fragments as the templates with the primers swp3461-UF and swp3461-DR. After digestion with the restriction enzymes SmaI and KpnI, the treated fusion PCR products were ligated into the SmaI and KpnI sites of the suicide plasmid pRE112 (47), resulting in the mutagenesis vector pRE112-Δ*dmsE*. This vector was first introduced into *E. coli* WM3064 and then conjugated into the WP3 WT (wild type). Positive exconjugants were spread onto marine agar 2216E plates supplemented with 10% (wt/vol) sucrose. The chloramphenicol-sensitive and sucrose-resistant colonies were screened by PCR for the *dmsE* deletion. The Δ*dmsA1* Δ*dmsE* and Δ*dmsA6* Δ*dmsE* double mutants were constructed by introducing pRE112-Δ*dmsE* into the Δ*dmsA1* and Δ*dmsA6* mutant strains, respectively. To construct the complemented strains of the Δ*dmsB1* Δ*dmsB6* (ΔΔ*dmsB*) mutant for subcellular localization experiments, the intact *dmsB1* and *dmsB6* gene fragments were amplified from the WP3 wild-type genomic DNA. The resulting PCR products were fused to a 3×HA epitope tag from hemagglutinin of human influenza A virus (HA tag) on the C terminus of DmsB and then inserted into the shuttle vector pSW2, which was developed from the filamentous phage SW1 of WP3 (48). The ΔΔ*dmsB-dmsB1*-3HA and ΔΔ*dmsB-dmsB6*-3HA strain transformants were obtained by introducing the recombinant plasmids pSW2-*dmsB1*-3HA and pSW2-*dmsB6*-3HA, respectively, into the ΔΔ*dmsB* mutant strain via conjugation.

RNA extraction and qRT-PCR. WP3 total RNA was isolated using TRIzol reagent (Molecular Research Center, Inc., Cincinnati, OH) according to the manufacturer's recommendations with modifications (49). Briefly, 2 ml of mid-log-phase cultures (2×10^7 cells/ml or OD_{600} of ~0.2) was harvested by centrifugation and homogenized in 1 ml of TRIzol, and 200 μl of chloroform was added. After brief vortexing, the samples were centrifuged at 12,000 × *g* for 15 min at 4°C. The upper aqueous phase was transferred to a tube containing an equal volume of isopropanol (500 μl). The mixtures were thoroughly vortexed and centrifuged at 12,000 × *g* for 20 min at 4°C. Supernatants were discarded, and the precipitated RNA pellets were then washed twice with 1 ml of 75% ethanol. After removing residual genomic DNA, all RNA samples were resuspended in 30 μl of RNase-free water, followed by a reverse transcription reaction with the RevertAid first strand cDNA synthesis kit (Thermo Scientific, Lithuania) to obtain cDNA. Quantitative real-time PCR (qRT-PCR) assays were performed in triplicate for each sample, and the mean values and standard deviations were calculated for the relative RNA expression levels (50).

DMSO concentration analysis. Aliquots (0.5 ml) of the culture recovered at different time points were filtered immediately through 0.22-μm Millex-GP filters (Millipore, Carrigtwohill, Ireland) and stored at −70°C prior to use. DMSO concentration analysis was performed as previously reported (21). Briefly, after 10-fold dilution with distilled water, the samples were analyzed on an Agilent 1200 series (Agilent Technologies, Santa Clara, CA, USA) high-performance liquid chromatography (HPLC) system with a diode-array detector (DAD) at 210 nm. DMSO was separated using an Aminex HPX-87H sulfonic column (Bio-Rad, Hercules, CA, USA) at 50°C with 5 mmol H_2SO_4 as the mobile phase at a flow rate of 0.5 ml min^{-1}. Commercially available DMSO (Sigma-Aldrich, St. Louis, Mo, USA) was used to generate a calibration curve to calculate the concentration of DMSO. The calibration curve was linear ($R^2 = 1.000$) over a concentration range of 0.05 to 10 mM.

Phylogenetic analysis. DmsA protein sequences were obtained from the NCBI GenPept database using the BLASTP suite. Swp3459 (DmsA1) and Swp0724 (DmsA6) sequences were used as queries. Sequences with identities of ≥42% (E value = 0) were chosen as significantly similar. The phylogenetic tree (Fig. 1) of 44 DmsA protein sequences from *Shewanella* and other gammaproteobacteria was constructed using the maximum likelihood method from FastTree version 2.1.3 (JTT model, CAT approximation) (51), and the trimethylamine *N*-oxide (TMAO) reductase (TorA) of *Vibrio cholerae* 2012EL-2176 was used as the outgroup. For each data set, bootstrap values were obtained with 1,000 replicates.

Preparation of ultrathin sections of bacterial cells. WP3 strains grown under different conditions were harvested by centrifugation and then treated with 4% (vol/vol) glutaraldehyde in phosphate-buffered saline (PBS) overnight at 4°C. Fixed cells were collected, washed three times with 0.1 M phosphate buffer (PB, pH 7.4) for 15 min, and postfixed in prechilled 1% osmic acid at 4°C for 2 h. The cells were dehydrated in a series of concentrations of alcohol (50%, 70%, 90%) for 10 min at each concentration. Subsequently, the fixed cells were permeated and embedded in epoxy resin (52). The samples were sectioned to yield 70-nm ultrathin sections with an Ultracut UC-6 microtome (Leica, Heidelberg, Germany). These sections were transferred to carbon-coated copper grids and dried under ambient conditions.

Immunogold labeling and transmission electron microscopy. For immunogold labeling of ultrathin sections, the sections on the grids were immersed in 0.01 M phosphate-buffered saline (PBS) solution containing 0.02 M glycine to block nonspecific labeling. These sections were then incubated with mouse anti-HA monoclonal antibody (clone HA-7; Sigma-Aldrich, St. Louis, MO) for 1 h (1:500 dilutions), washed with PBS three times for 5 min, incubated with gold-conjugated anti-mouse IgG (10-nm-diameter gold nanoparticles; Sigma-Aldrich, St. Louis, MO) for 1 h (1:50 dilutions), and washed six times with PBS (5 min each wash). To increase contrast, the ultrathin sections were stained with platinum blue (TI-blue; Nisshin EM Corporation, Tokyo, Japan) and lead citrate and then observed using a Tecnai G2 Spirit BioTwin (120 kV) transmission electron microscope (TEM) (FEI Company, Eindhoven, The Netherlands). A similar procedure was applied for immunogold labeling of whole bacteria. Whole bacteria were not stained with platinum blue or lead citrate solutions to enable observation of the gold

TABLE 3 Primers used in this study

Primers	Primer sequence (5′-3′)[a]	Description
Mutation use		
swp0724-UF	TTGAGCTCCGAGGTAACGCAAAATGAAAAGAC	Deleting *dmsA6*
swp0724-UR	CCTTTAGTAGTAGTACGCGCCAGTGCCATAAA	Deleting *dmsA6*
swp0724-DF	GTACTACTACTAAAGGCCGCACCCACTCA	Deleting *dmsA6*
swp0724-DR	TTGCATGCGAAACTGCCACCAACAAACTCATA	Deleting *dmsA6*
swp0725-UF	TAGAGCTCATGTCGATACGGATTACCCACTG	Deleting *dmsB6*
swp0725-UR	TTTGCCATATAAACGCGACGCTGAATAATACC	Deleting *dmsB6*
swp0725-DF	GCGTTTATATGGCAAAGGCGATACTCACC	Deleting *dmsB6*
swp0725-DR	AAGCATGCGCTCTGTTAATTTTTCGTCGTTCC	Deleting *dmsB6*
swp3459-UF	TACCCGGGTGTTATCTTGCGGGTTGCTATTGT	Deleting *dmsA1*
swp3459-UR	TATACCGCTGCCGTTAAGGTTCGTATCACTCC	Deleting *dmsA1*
swp3459-DF	TAACGGCAGCGGTATAACATTGGCATCATCAG	Deleting *dmsA1*
swp3459-DR	ATTCTAGAAGTAATACCGGAGTCAGCCCTTCT	Deleting *dmsA1*
swp3458-UF	AAGGTACCCGGCCTCTGGATGACGAATAAG	Deleting *dmsB1*
swp3458-UR	GTGAATGGAGTACGGCGACGGCGATGGA	Deleting *dmsB1*
swp3458-DF	GCCGTACTCCATTCACCGCCACCGTATTCAT	Deleting *dmsB1*
swp3458-DR	AAGAGCTCTGCCGTTAAGGTTCGTATCACTCC	Deleting *dmsB1*
swp3460-UF	AACCCCCGGGTAATGAAACCTGTGCCGAGTG	Deleting *dmsF*
swp3460-UR	GAGTGTCACATCATCGGCATCAACAGCAC	Deleting *dmsF*
swp3460-DF	CGATGATGTGACACTCGGCATGGACTAC	Deleting *dmsF*
swp3460-DR	TAGAGGTACCGCCTGTAACTGTTGCTGCAC	Deleting *dmsF*
swp3461-UF	GTACCCGGGAGTATAGGCAAACTATATGCAA	Deleting *dmsE*
swp3461-UR	GGCACACGGAAGAGTATTTACCTTCGCTA	Deleting *dmsE*
swp3461-DF	TACTCTTCCGTGTGCCGCAATTATGTCA	Deleting *dmsE*
swp3461-DR	GCACGGTACCTACCAGAATAGCCATCAGTCG	Deleting *dmsE*
swp4806-UF	AAGGTACCCCTCCTAAATCTGACCG	Deleting *cymA*
swp4806-UR	CAGTTAAGGGTGTTGCTCACGTTTACCCAAAG	Deleting *cymA*
swp4806-DF	GCAACACCCTTAACTGGGTTGTGCGGTAAGTG	Deleting *cymA*
swp4806-DR	AATCTAGAGAGAGAGTTAGAGCCATGTCTCAT	Deleting *cymA*
ChlFor	TATCACTTATTCAGGCGTAGCA	Identifying chloramphenicol resistance gene in suicide plasmid pRE112
ChlRev	CCCAACACCGGACAAAAAGGA	
Complementation use		
cymA-F	CGGGATCCAGACCCACCTTTTGAGGAAA	Complement *cymA*
cymA-R	CCGCTCGAGTCCACTTCTGCTTTGCATTG	
Subcellular location		
(P+3458)F	CTTACTCGAGGTTGTTTCTAGTTGTATCTC	*dmsB1* amplification
(P+3458)R	TATGGGTAAACCTCAGATGGGTTTAAAATGCT	*dmsB1* amplification
3458HAF	CTGAGGTTTACCCATACGATGTTCCAGATTACG	3×HA amplification
3458HAR	CACAACGCGTGAGCTCGGTATTAAGCGTAA	3×HA amplification
P0724F	CTTACTCGAGTACCTTATAAAAACAGAGAGCC	*dmsB6* promoter
P0724R	TTAGTCATTTTGCGTTACCTCGACATTTA	*dmsB6* promoter
swp0725F	AACGCAAAATGACTAATTTAATTCAAACAACC	*dmsB6* amplification
swp0725R	TATGGGTAAACCTCAGATGGGTTTAAAATGCT	*dmsB6* amplification
0725HAF	TTATTAATAGCAGAGAAGTTTACCCATACGATGTTCCAGATTACG	3×HA amplification
0725HAR	CACAACGCGTGAGCTCGGTATTAAGCGTAA	3×HA amplification
qRT-PCR use		
dmsA1 For	AGGCTGTAATTCTAGCTCTGATGATG	qRT-PCR
dmsA1 Rev	AAGCACGATGACCAGGTTACCT	qRT-PCR
dmsB1 For	GAAGACATTTGTATCGGTTGTGAAA	qRT-PCR
dmsB1 Rev	GCGTTCACGGTCAATTTGC	qRT-PCR
dmsG1 For	ACCGATAATCAAGCGTTAGT	qRT-PCR
dmsG1 Rev	AAGTCACTGCTGCTATGG	qRT-PCR
dmsH1 For	GCAATGGAGTAAGTCAATTCT	qRT-PCR
dmsH1 Rev	CCGCTATGGTGTTAGTGA	qRT-PCR
dmsA6 For	GATGACAAATGTATCGGCTGTAATATG	qRT-PCR
dmsA6 Rev	TTTTTACGCTCAGTATCCATTTGC	qRT-PCR
dmsB6 For	CACTGCAGTTGGTGGGATACC	qRT-PCR
dmsB6 Rev	CGTAGCCATGGCACATTATGA	qRT-PCR
dmsG6 For	AGTCAGCACATTGAGTCA	qRT-PCR
dmsG6 Rev	TCAGCAGTTCTCTTAGTAACA	qRT-PCR
dmsH6 For	TTGCCGAAGAGGTTGTAA	qRT-PCR
dmsH6 Rev	TCATTGAGGTTGCTTCTAATAG	qRT-PCR
swp2079 For	TTAAGGCAATGGAAGCTGCAT	Reference gene
swp2079 Rev	CGTCTTTACCCGTTAATGATACGA	*swp2079* primer pairs

[a]The restriction sites included in the PCR primers are underlined.

particles on the whole surface of the bacteria by TEM (19). Negative controls were performed by omitting the incubation with the primary antibody. For statistical analysis, the numbers of gold particles along the cell membrane structures were counted for 50 fields for ultrathin sections prepared from each tested WP3 strain (53).

SUPPLEMENTAL MATERIAL

Supplemental material for this article may be found at https://doi.org/10.1128/AEM.01262-17.

SUPPLEMENTAL FILE 1, PDF file, 1.1 MB.

ACKNOWLEDGMENTS

This work was financially supported by the National Natural Science Foundation of China (grant 31290232), the China Ocean Mineral Resources R & D Association (grant DY125-22-04), and the National Natural Science Foundation of China (grants 41530967 and 41676118).

REFERENCES

1. Lee PA, de Mora SJ, Levasseur M. 1999. A review of dimethylsulfoxide in aquatic environments. Atmos-Ocean 37:439–456. https://doi.org/10.1080/07055900.1999.9649635.
2. Hatton AD, Darroch L, Malin G. 2005. The role of dimethylsulphoxide in the marine biogeochemical cycle of dimethylsulphide. Oceanogr Mar Biol 42:29–56.
3. Moran MA, Reisch CR, Kiene RP, Whitman WB. 2012. Genomic insights into bacterial DMSP transformations. Annu Rev Mar Sci 4:523–542. https://doi.org/10.1146/annurev-marine-120710-100827.
4. Simó R. 1998. Trace chromatographic analysis of dimethyl sulfoxide and related methylated sulfur compounds in natural waters. J Chromatogr A 807:151–164. https://doi.org/10.1016/S0021-9673(98)00086-7.
5. Hatton AD, Malin G, Turner S, Liss PS. 1996. DMSO, p 405–412. *In* Keller MD, Kiene RP, Kirst GO, Visscher PT (ed), Biological and environmental chemistry of DMSP and related sulfonium compounds. Springer, New York, NY.
6. Asher EC, Dacey JW, Mills MM, Arrigo KR, Tortell PD. 2011. High concentrations and turnover rates of DMS, DMSP and DMSO in Antarctic sea ice. Geophys Res Lett 38:L23609. https://doi.org/10.1029/2011GL049712.
7. Sunda W, Kieber DJ, Kiene RP, Huntsman S. 2002. An antioxidant function for DMSP and DMS in marine algae. Nature 418:317–320. https://doi.org/10.1038/nature00851.
8. Hatton AD, Malin G, Liss PS. 1999. Distribution of biogenic sulphur compounds during and just after the southwest monsoon in the Arabian Sea. Deep Sea Res Part II 46:617–632. https://doi.org/10.1016/S0967-0645(98)00120-9.
9. Hatton AD, Turner S, Malin G, Liss PS. 1998. Dimethylsulphoxide and other biogenic sulphur compounds in the Galapagos Plume. Deep Sea Res Part II 45:1043–1053. https://doi.org/10.1016/S0967-0645(98)00017-4.
10. Süss J, Herrmann K, Seidel M, Cypionka H, Engelen B, Sass H. 2008. Two distinct *Photobacterium* populations thrive in ancient Mediterranean sapropels. Microb Ecol 55:371–383. https://doi.org/10.1007/s00248-007-9282-6.
11. Xiao X, Wang P, Zeng X, Bartlett DH, Wang F. 2007. *Shewanella psychrophila* sp. nov. and *Shewanella piezotolerans* sp. nov., isolated from west Pacific deep-sea sediment. Int J Syst Evol Microbiol 57:60–65. https://doi.org/10.1099/ijs.0.64500-0.
12. McCrindle SL, Kappler U, McEwan AG. 2005. Microbial dimethylsulfoxide and trimethylamine-*N*-oxide respiration. Adv Microb Physiol 50:147–198, 199e–201e. https://doi.org/10.1016/S0065-2911(05)50004-3.
13. Lubitz SP, Weiner JH. 2003. The *Escherichia coli ynfEFGHI* operon encodes polypeptides which are paralogues of dimethyl sulfoxide reductase (DmsABC). Arch Biochem Biophys 418:205–216. https://doi.org/10.1016/j.abb.2003.08.008.
14. Stanley NR, Sargent F, Buchanan G, Shi J, Stewart V, Palmer T, Berks BC. 2002. Behaviour of topological marker proteins targeted to the Tat protein transport pathway. Mol Microbiol 43:1005–1021. https://doi.org/10.1046/j.1365-2958.2002.02797.x.
15. Hau HH, Gralnick JA. 2007. Ecology and biotechnology of the genus *Shewanella*. Annu Rev Microbiol 61:237–258. https://doi.org/10.1146/annurev.micro.61.080706.093257.
16. Fredrickson JK, Romine MF, Beliaev AS, Auchtung JM, Driscoll ME, Gardner TS, Nealson KH, Osterman AL, Pinchuk G, Reed JL, Rodionov DA, Rodrigues JL, Saffarini DA, Serres MH, Spormann AM, Zhulin IB, Tiedje JM. 2008. Towards environmental systems biology of *Shewanella*. Nat Rev Microbiol 6:592–603. https://doi.org/10.1038/nrmicro1947.
17. Venkateswaran K, Moser DP, Dollhopf ME, Lies DP, Saffarini DA, MacGregor BJ, Ringelberg DB, White DC, Nishijima M, Sano H, Burghardt J, Stackebrandt E, Nealson KH. 1999. Polyphasic taxonomy of the genus *Shewanella* and description of *Shewanella oneidensis* sp. nov. Int J Syst Bacteriol 49:705–724. https://doi.org/10.1099/00207713-49-2-705.
18. Coursolle D, Gralnick JA. 2010. Modularity of the Mtr respiratory pathway of *Shewanella oneidensis* strain MR-1. Mol Microbiol 77:995–1008.
19. Gralnick JA, Vali H, Lies DP, Newman DK. 2006. Extracellular respiration of dimethyl sulfoxide by *Shewanella oneidensis* strain MR-1. Proc Natl Acad Sci U S A 103:4669–4674. https://doi.org/10.1073/pnas.0505959103.
20. Wang F, Wang P, Chen M, Xiao X. 2004. Isolation of extremophiles with the detection and retrieval of *Shewanella* strains in deep-sea sediments from the west Pacific. Extremophiles 8:165–168. https://doi.org/10.1007/s00792-003-0365-0.
21. Xiong L, Jian H, Zhang Y, Xiao X. 2016. The two sets of DMSO respiratory systems of *Shewanella piezotolerans* WP3 are involved in deep sea environmental adaptation. Front Microbiol 7:1418. https://doi.org/10.3389/fmicb.2016.01418.
22. Pitts KE, Dobbin PS, Reyes-Ramirez F, Thomson AJ, Richardson DJ, Seward HE. 2003. Characterization of the *Shewanella oneidensis* MR-1 decaheme cytochrome MtrA: expression in *Escherichia coli* confers the ability to reduce soluble Fe(III) chelates. J Biol Chem 278:27758–27765. https://doi.org/10.1074/jbc.M302582200.
23. Yayanos AA, Van Boxtel R. 1982. Coupling device for quick high-pressure connections to 100 MPa. Rev Sci Instrum 53:704–705. https://doi.org/10.1063/1.1137011.
24. Gross R, Eichler R, Simon J. 2005. Site-directed modifications indicate differences in axial haem *c* iron ligation between the related NrfH and NapC families of multihaem *c*-type cytochromes. Biochem J 390:689–693. https://doi.org/10.1042/BJ20050448.
25. Myers CR, Myers JM. 1997. Cloning and sequence of *cymA*, a gene encoding a tetraheme cytochrome *c* required for reduction of iron(III), fumarate, and nitrate by *Shewanella putrefaciens* MR-1. J Bacteriol 179:1143–1152. https://doi.org/10.1128/jb.179.4.1143-1152.1997.
26. Szeinbaum N, Burns JL, DiChristina TJ. 2014. Electron transport and protein secretion pathways involved in Mn(III) reduction by *Shewanella oneidensis*. Environ Microbiol Rep 6:490–500. https://doi.org/10.1111/1758-2229.12173.
27. Coursolle D, Gralnick JA. 2012. Reconstruction of extracellular respiratory pathways for iron(III) reduction in *Shewanella oneidensis* strain MR-1. Front Microbiol 3:56. https://doi.org/10.3389/fmicb.2012.00056.
28. Hartshorne RS, Reardon CL, Ross D, Nuester J, Clarke TA, Gates AJ, Mills PC, Fredrickson JK, Zachara JM, Shi L, Beliaev AS, Marshall MJ, Tien M, Brantley S, Butt JN, Richardson DJ. 2009. Characterization of an electron conduit between bacteria and the extracellular environment. Proc Natl

Acad Sci U S A 106:22169–22174. https://doi.org/10.1073/pnas.0900086106.
29. Weiner JH, Rothery RA, Sambasivarao D, Trieber CA. 1992. Molecular analysis of dimethylsulfoxide reductase: a complex iron-sulfur molybdoenzyme of *Escherichia coli*. Biochim Biophys Acta 1102:1–18. https://doi.org/10.1016/0005-2728(92)90059-B.
30. Cordova CD, Schicklberger MF, Yu Y, Spormann AM. 2011. Partial functional replacement of CymA by SirCD in *Shewanella oneidensis* MR-1. J Bacteriol 193:2312–2321. https://doi.org/10.1128/JB.01355-10.
31. Jin M, Zhang Q, Sun Y, Gao H. 2016. NapB in excess inhibits growth of *Shewanella oneidensis* by dissipating electrons of the quinol pool. Sci Rep 6:37456. https://doi.org/10.1038/srep37456.
32. David NA. 1972. The pharmacology of dimethyl sulfoxide. Annu Rev Pharmacol 12:353–374. https://doi.org/10.1146/annurev.pa.12.040172.002033.
33. McEwan A, Wetzstein H, Meyer O, Jackson J, Ferguson S. 1987. The periplasmic nitrate reductase of *Rhodobacter capsulatus*; purification, characterisation and distinction from a single reductase for trimethylamine-*N*-oxide, dimethylsulphoxide and chlorate. Arch Microbiol 147:340–345. https://doi.org/10.1007/BF00406130.
34. Kappler U, Schäfer H. 2014. Transformations of dimethylsulfide, p 279–313. *In* Kroneck PMH, Sosa Torres ME (ed), The metal-driven biogeochemistry of gaseous compounds in the environment. Springer, New York, NY.
35. Yano Y, Nakayama A, Ishihara K, Saito H. 1998. Adaptive changes in membrane lipids of barophilic bacteria in response to changes in growth pressure. Appl Environ Microbiol 64:479–485.
36. Hazel JR, Williams E. 1990. The role of alterations in membrane lipid composition in enabling physiological adaptation of organisms to their physical environment. Prog Lipid Res 29:167–227. https://doi.org/10.1016/0163-7827(90)90002-3.
37. Paynter S, Cooper A, Gregory L, Fuller B, Shaw R. 1999. Permeability characteristics of human oocytes in the presence of the cryoprotectant dimethylsulphoxide. Hum Reprod 14:2338–2342. https://doi.org/10.1093/humrep/14.9.2338.
38. Liu J, Zieger M, Lakey J, Woods E, Critser J. 1997. Water and DMSO permeability at 22°C, 5°C, and −3°C for human pancreatic islet cells. Transplant Proc 29:1987. https://doi.org/10.1016/S0041-1345(97)00198-X.
39. Shi L, Deng S, Marshall MJ, Wang Z, Kennedy DW, Dohnalkova AC, Mottaz HM, Hill EA, Gorby YA, Beliaev AS, Richardson DJ, Zachara JM, Fredrickson JK. 2008. Direct involvement of type II secretion system in extracellular translocation of *Shewanella oneidensis* outer membrane cytochromes MtrC and OmcA. J Bacteriol 190:5512–5516. https://doi.org/10.1128/JB.00514-08.
40. DiChristina TJ, Moore CM, Haller CA. 2002. Dissimilatory Fe(III) and Mn(IV) reduction by *Shewanella putrefaciens* requires *ferE*, a homolog of the *pulE* (*gspE*) type II protein secretion gene. J Bacteriol 184:142–151. https://doi.org/10.1128/JB.184.1.142-151.2002.
41. Filloux A. 2010. Secretion signal and protein targeting in bacteria: a biological puzzle. J Bacteriol 192:3847–3849. https://doi.org/10.1128/JB.00565-10.
42. Korotkov KV, Sandkvist M, Hol WG. 2012. The type II secretion system: biogenesis, molecular architecture and mechanism. Nat Rev Microbiol 10:336–351.
43. Sandkvist M. 2001. Biology of type II secretion. Mol Microbiol 40:271–283. https://doi.org/10.1046/j.1365-2958.2001.02403.x.
44. Chen Y, Wang F, Xu J, Mehmood MA, Xiao X. 2011. Physiological and evolutionary studies of NAP systems in *Shewanella piezotolerans* WP3. ISME J 5:843–855. https://doi.org/10.1038/ismej.2010.182.
45. Wang F, Wang J, Jian H, Zhang B, Li S, Wang F, Zeng X, Gao L, Bartlett DH, Yu J, Hu S, Xiao X. 2008. Environmental adaptation: genomic analysis of the piezotolerant and psychrotolerant deep-sea iron reducing bacterium *Shewanella piezotolerans* WP3. PLoS One 3:e1937. https://doi.org/10.1371/journal.pone.0001937.
46. Allen EE, Facciotti D, Bartlett DH. 1999. Monounsaturated but not polyunsaturated fatty acids are required for growth of the deep-sea bacterium *Photobacterium profundum* SS9 at high pressure and low temperature. Appl Environ Microbiol 65:1710–1720.
47. Edwards RA, Keller LH, Schifferli DM. 1998. Improved allelic exchange vectors and their use to analyze 987P fimbria gene expression. Gene 207:149–157. https://doi.org/10.1016/S0378-1119(97)00619-7.
48. Yang X, Jian H, Wang F. 2015. pSW2, a novel low-temperature-inducible gene expression vector based on a filamentous phage of the deep-sea bacterium *Shewanella piezotolerans* WP3. Appl Environ Microbiol 81:5519–5526. https://doi.org/10.1128/AEM.00906-15.
49. Dussault AA, Pouliot M. 2006. Rapid and simple comparison of messenger RNA levels using real-time PCR. Biol Proced Online 8:1–10. https://doi.org/10.1251/bpo114.
50. Jian H, Xiong L, Xu G, Xiao X, Wang F. 2016. Long 5′ untranslated regions regulate the RNA stability of the deep-sea filamentous phage SW1. Sci Rep 6:21908. https://doi.org/10.1038/srep21908.
51. Price MN, Dehal PS, Arkin AP. 2010. FastTree 2–approximately maximum-likelihood trees for large alignments. PLoS One 5:e9490. https://doi.org/10.1371/journal.pone.0009490.
52. Rodríguez-Lorenzo L, Krpetic Z, Barbosa S, Alvarez-Puebla RA, Liz-Marzán LM, Prior IA, Brust M. 2011. Intracellular mapping with SERS-encoded gold nanostars. Integr Biol (Camb) 3:922–926. https://doi.org/10.1039/c1ib00029b.
53. Feng S, Li H, Tai Y, Huang J, Su Y, Abramowitz J, Zhu MX, Birnbaumer L, Wang Y. 2013. Canonical transient receptor potential 3 channels regulate mitochondrial calcium uptake. Proc Natl Acad Sci U S A 110:11011–11016. https://doi.org/10.1073/pnas.1309531110.
54. Siezen RJ, Wilson G. 2008. Unpublished but public microbial genomes with biotechnological relevance. Microb Biotechnol 1:202–207. https://doi.org/10.1111/j.1751-7915.2008.00034.x.
55. Caro-Quintero A, Auchtung J, Deng J, Brettar I, Höfle M, Tiedje JM, Konstantinidis KT. 2012. Genome sequencing of five *Shewanella baltica* strains recovered from the oxic-anoxic interface of the Baltic Sea. J Bacteriol 194:1236. https://doi.org/10.1128/JB.06468-11.
56. Nealson K, Myers C, Wimpee B. 1991. Isolation and identification of manganese-reducing bacteria and estimates of microbial Mn (IV)-reducing potential in the Black Sea. Deep Sea Res Part A 38:S907–S920. https://doi.org/10.1016/S0198-0149(10)80016-0.
57. Makemson JC, Fulayfil NR, Landry W, Van Ert LM, Wimpee CF, Widder EA, Case JF. 1997. *Shewanella woodyi* sp. nov., an exclusively respiratory luminous bacterium isolated from the Alboran Sea. Int J Syst Bacteriol 47:1034–1039. https://doi.org/10.1099/00207713-47-4-1034.
58. Fredrickson JK, Zachara JM, Kennedy DW, Dong H, Onstott TC, Hinman NW, Li S. 1998. Biogenic iron mineralization accompanying the dissimilatory reduction of hydrous ferric oxide by a groundwater bacterium. Geochim Cosmochim Acta 62:3239–3257. https://doi.org/10.1016/S0016-7037(98)00243-9.
59. Lee J, Gibson D, Shewan JM. 1977. A numerical taxonomic study of some *Pseudomonas*-like marine bacteria. J Gen Microbiol 98:439–451. https://doi.org/10.1099/00221287-98-2-439.
60. Zhao J, Manno D, Leggiadro C, O'Neil D, Hawari J. 2006. *Shewanella halifaxensis* sp. nov., a novel obligately respiratory and denitrifying psychrophile. Int J Syst Evol Microbiol 56:205–212. https://doi.org/10.1099/ijs.0.63829-0.
61. Myers CR, Nealson KH. 1988. Bacterial manganese reduction and growth with manganese oxide as the sole electron acceptor. Science 240:1319–1321. https://doi.org/10.1126/science.240.4857.1319.
62. Leonardo MR, Moser DP, Barbieri E, Brantner CA, MacGregor BJ, Paster BJ, Stackebrandt E, Nealson KH. 1999. *Shewanella pealeana* sp. nov., a member of the microbial community associated with the accessory nidamental gland of the squid *Loligo pealei*. Int J Syst Bacteriol 49:1341–1351. https://doi.org/10.1099/00207713-49-4-1341.
63. Obuekwe C, Westlake D. 1982. Effects of medium composition on cell pigmentation, cytochrome content, and ferric iron reduction in a *Pseudomonas* sp. isolated from crude oil. Can J Microbiol 28:989–992. https://doi.org/10.1139/m82-148.
64. Zhao J-S, Manno D, Beaulieu C, Paquet L, Hawari J. 2005. *Shewanella sediminis* sp. nov., a novel Na^+-requiring and hexahydro-1,3,5-trinitro-1,3,5-triazine-degrading bacterium from marine sediment. Int J Syst Evol Microbiol 55:1511–1520. https://doi.org/10.1099/ijs.0.63604-0.
65. Gao H, Yang ZK, Wu L, Thompson DK, Zhou J. 2006. Global transcriptome analysis of the cold shock response of *Shewanella oneidensis* MR-1 and mutational analysis of its classical cold shock proteins. J Bacteriol 188:4560–4569. https://doi.org/10.1128/JB.01908-05.